



How to expand the cooling capacity of blue and green spaces in peri-urban areas throughout the entire diurnal cycle: Evidence from an inland multilake city



Wei Ding ^{a,b,c}, Mengyang Liu ^{a,b,c}, Yunni Wu ^{a,b,c}, Hong Chen ^{a,b,c,*}

^a School of Architecture and Urban Planning, Huazhong University of Science and Technology, Wuhan, 430074, China

^b Hubei Engineering and Technology Research Center of Urbanization, Wuhan, 430074, China

^c The Key Laboratory of Urban Simulation for Ministry of Natural Resources, Wuhan, 430074, China

ARTICLE INFO

Handling Editor: Cecilia Maria Villas Bôas de Almeida

Keywords:

Urban sprawl
blue-green space
Urban form
Cool island
WRF-UCM

ABSTRACT

Blue and green spaces (BGs) play a critical role in mitigating the urban heat island effect, especially during heatwaves. However, limited research has been conducted on the impact of urban form factors on the cooling effect of BGs throughout the entire diurnal cycle. This study aimed to evaluate the cooling capacity of BGs in Wuhan, China, by considering the cooling distance (ΔL_{max}) and cooling intensity (ΔT_{max}) via the WRF-UCM model, considering the internal land use changes and spatial changes within the adjacent spaces of the BGs. The findings are as follows: 1) the BGs have a maximum ΔT_{max} (1.44 °C) and ΔL_{max} (2.15 km) during the daytime, which are reduced by 18.6 % and 85.4 %, respectively, at night; 2) during the daytime period, no green space within the BGs results in a greater ΔT_{max} and ΔL_{max} , while the law of diminishing marginal utility (LDMU) is disrupted by the disappearance of green spaces at night; and 3) open high-rise patterns show a larger ΔT_{max} and ΔL_{max} and lower T_{mean} in the daytime, with a smaller ΔL_{max} and higher T_{mean} at night. The diurnal T_{mean} is consistently lower for the greening strategy. High-rise and low-density patterns can expand the BG cooling capacity, but they bring new heat waves at night.

1. Introduction

Rapid urbanization has led to the inevitable expansion of urban areas and population growth. Research indicates that uncontrolled land development can worsen the urban microclimate (Zhang and Gu, 2013, Zhang et al., 2021; Hong et al., 2023; Liu et al., 2023). The construction of urban ventilation corridors has to some extent improved the quality of the outdoor microclimate in cities (Ren et al., 2018; Fang and Zhao, 2022). However, some scholars have found that urban expansion has dominated overall urban warming (Cao et al., 2022), and the climate mitigation capacity of some local-scale spatial planning approaches is only minimally effective. The disorderly nature of urban spatial structure is likely to dominate the deterioration of the urban climate. Spontaneous construction on the periphery of a city is likely to increase surface roughness and create new thermal agglomerations, reducing near-surface wind speeds and horizontal convection (Li et al., 2022). The climate-regulating role of blue space and green space in urban fringe areas is likely to be diminished.

Blue and green space (BG) is important for establishing ventilation corridors, and its enormous potential for mitigating heatwaves and microclimate issues has been widely recognized. Wong et al. investigated the cooling benefits of urban parks in Singapore through field measurements (Wong and Yu, 2005; Yu and Hien, 2006). Ghosh and Das examined the effect of the shapes of green spaces and water bodies on the range of peripheral surface temperature control in Kolkata, a megacity in India (Ghosh and Das, 2018). Wang et al. used the ENVI-MET model to evaluate the potential for heat island mitigation by neighbourhood vegetative (tree and grass) in Toronto, Canada (Wang et al., 2016). Several scholars have also developed empirical models based on data from actual measurements, modelling and other literature in 100 cities worldwide and found that irrigated green space can provide cooling benefits to more than 9/10 of cities, especially in arid areas (Cheung et al., 2021). The Chinese government is actively seeking nature-based solutions to urban climate deterioration. In August 2023, the Chinese Ministry of Ecology and Environment issued a pilot notice on deepening climate-adaptive urban construction. We propose exploring spatial planning adaptation and mitigation strategies for

* Corresponding author. School of Architecture and Urban Planning, Huazhong University of Science and Technology, Wuhan, 430074, China.

E-mail address: chhwh@hust.edu.cn (H. Chen).

Nomenclature

BGs	Blue and green spaces
LDMU	Law of Diminishing Marginal Utility
WRF-UCM	Weather Research & Forecasting Model coupled with urban canyon parameters
LST	Land surface temperature
BD	Building density
BH	Building height
FAR	Floor area ratio
ΔT_{max}	The temperature difference between the first turning point and the BGs boundary
ΔL_{max}	The distance between the first turning point and the BGs boundary
Tmean	The mean temperature of 10 buffers in the BGs adjacent space

climate change based on urban blue and green boundaries. In fact, Chinese scholars have been conducting extensive research on the microclimate benefits of BGs for many years. Yu et al. defined concepts such as the extent, intensity, and efficiency of urban cooling islands (UCIs), as well as the threshold value of efficiency (TVoE). They proposed the *law of diminishing marginal utility (LDMU)* and used remote sensing inversion methods to evaluate the cooling capacity of urban green spaces in the surrounding environment based on the first turning point of daytime land surface temperature (LST) around the green spaces (Yu et al., 2017). Subsequently, many scholars have applied remote sensing methods to assess the LDMU phenomenon near city BGs (Ouyang et al., 2020; Peng et al., 2021; Yao et al., 2022). Some scholars have focused on the benefits of microclimate margins for green spaces (Sun et al., 2012; Yu et al., 2020; Feng et al., 2022). Cai et al. compared the margin benefit of blue space in 34 cities in China by using remote sensing inversion of the LST. They analysed the city-water layout and used a fitted third-order polynomial function to characterize the cooling distance (ΔL_{max}) and the maximum temperature difference (ΔT_{max}) around water bodies (Cai et al., 2022). Shi et al. also used a similar approach to investigate the cooling conditions around green spaces in major cities in China. The authors discussed the correlations among park characteristics such as park shape, water body ratio, and the normalized difference vegetation index (NDVI) and the park cooling area (PCA), park cooling efficiency (PCE), park cooling intensity (PCI), and park cooling gradient (PCG) (Shi et al., 2023). In these studies, the first inflection point was commonly used as a reference, and the cooling distance and cooling intensity were used as indicators to accurately calculate the impact of BGs on the cooling capacity.

Urban form factors significantly influence the cooling capacity of BGs. Bernard et al. used the computational fluid dynamics software Code_Saturne to conduct a parameter study and found that a larger aspect ratio can increase the park cooling area (Bernard et al., 2018). Zhang et al. found that the building density (BD) and floor area ratio (FAR) in the built-up area surrounding BGs in the Xi'an area have an impact on the cooling capacity of green spaces. They also identified the optimal range of indicators that promote the expansion of the BG cooling capacity (Zhang et al., 2022). Fei et al. discussed the sea cooling capacity and reported that the distance needed for seawater cooling is approximately 2.5 km. They also identified anthropogenic heat and BD as key urban planning elements that influence the cooling effect of the sea (Guo et al., 2023). Zhou et al. used the WRF-UCM model to evaluate the impacts of BD and FAR on urban water bodies (Zhou et al., 2022). As peri-urban parks serve as excellent ventilation corridors for supplying cool and fresh air to city centres, it is crucial to find a balance between urban spatial expansion and heat mitigation in city centres. The spatial layout of adjacent BGs plays a vital role in achieving this dual objective.

Although many studies have investigated the factors influencing the cooling capacity of BGs, studies quantifying the effects of urban form mitigation strategies on the BG cooling capacity throughout the entire diurnal cycle are lacking, especially within BG-adjacent spaces. Indeed, climate assessments of night-time development and construction should not be overlooked. The urban energy balance follows a 24-h cycle, and the external heat exchange should be evaluated considering land use and spatial patterns observed during both day and night. Different urban forms may exhibit significant differences in heat dissipation at night (Mohan et al., 2013; Ren et al., 2023), and park water bodies may not contribute favourably to night-time cooling in urban areas (Yao et al., 2023).

Therefore, following the “adjacent space” concept in our previous work (Wu and Chen, 2023), spatial planning strategies that can enhance the diurnal cooling capacity during the day and night in BGs in peri-urban areas are explored in this paper. The research framework is shown in Fig. 1 and includes the following three steps: 1) utilize ECOSTRESS LST data to analyse the spatial distribution of nocturnal LSTs in Wuhan city and examine the LDMU phenomenon within the adjacent space of blue and green space (BG); 2) investigate the impact of peri-urban building height (BH) and BD on the cooling capacity of BG under constant FAR; and 3) analyse the effects of two developmental patterns (open high-rise and compact low-rise) and variations in green coverage within the adjacent space of BG. One main takeaway from this paper is that focusing on the different diurnal impacts of blue-green space cooling benefits and spatial planning can help provide more precise guidelines for microclimate regulation strategies.

2. Methodology

2.1. Study area

Wuhan city has a humid subtropical monsoon climate and is a typical water network city in inland China. In 2020, there were a total of 166 lakes in the city (<http://swj.wuhan.gov.cn/>). Over the past decade, Wuhan city has undergone rapid urbanization, with a continuous increase in population and a significant expansion of the built-up area. Compared with that in 2010, the permanent population of Wuhan city in 2020 was 12.3265 million, representing a growth of 26 %. The built-up area in 2020 was 885.11 km², an increase of 77 % compared to that in 2010. Urbanization has led to the phenomenon of urban heat islands and rapid deterioration of city air quality. As early as 2009, Wuhan city formulated the *Wuhan Urban Master Plan (2009–2020)*, which fully utilized the six ecological green wedges rich in lakes and green spaces to reduce temperature, leveraging Wuhan's unique geographical advantage. According to *Wuhan Territorial and Spatial Planning (2021–2035)*, the six green wedges have been incorporated into the city's spatial structure. However, the development and construction of these green wedges lack specific and explicit control recommendations. Therefore, this study focused on the development and construction of six green wedges in Wuhan city and discussed the practical significance of the space adjacent to the BGs. The study area is shown in Fig. 2.

2.2. ECOSTRESS LST

To determine the relationship between the night-time temperature distribution and the distance around the BGs, we need the night-time LST data for empirical analysis. Currently, obtaining LST data for urban areas at night is quite challenging. Fortunately, ECOSTRESS LST products have made it possible to obtain night-time urban LSTs, and their accuracy has been verified and proven by scholars (Han et al., 2023; Wang et al., 2023). The article utilizes the ECOSTRESS Tiled Land Surface Temperature and Emissivity Instantaneous L2 Global 70 m V002 (ECO_L2T_LSTE.002) product, which provides GeoTIFF format files that can be directly visualized in ArcGIS. Although ECOSTRESS was launched in 2018 (Fisher et al., 2020), the available period in the Wuhan

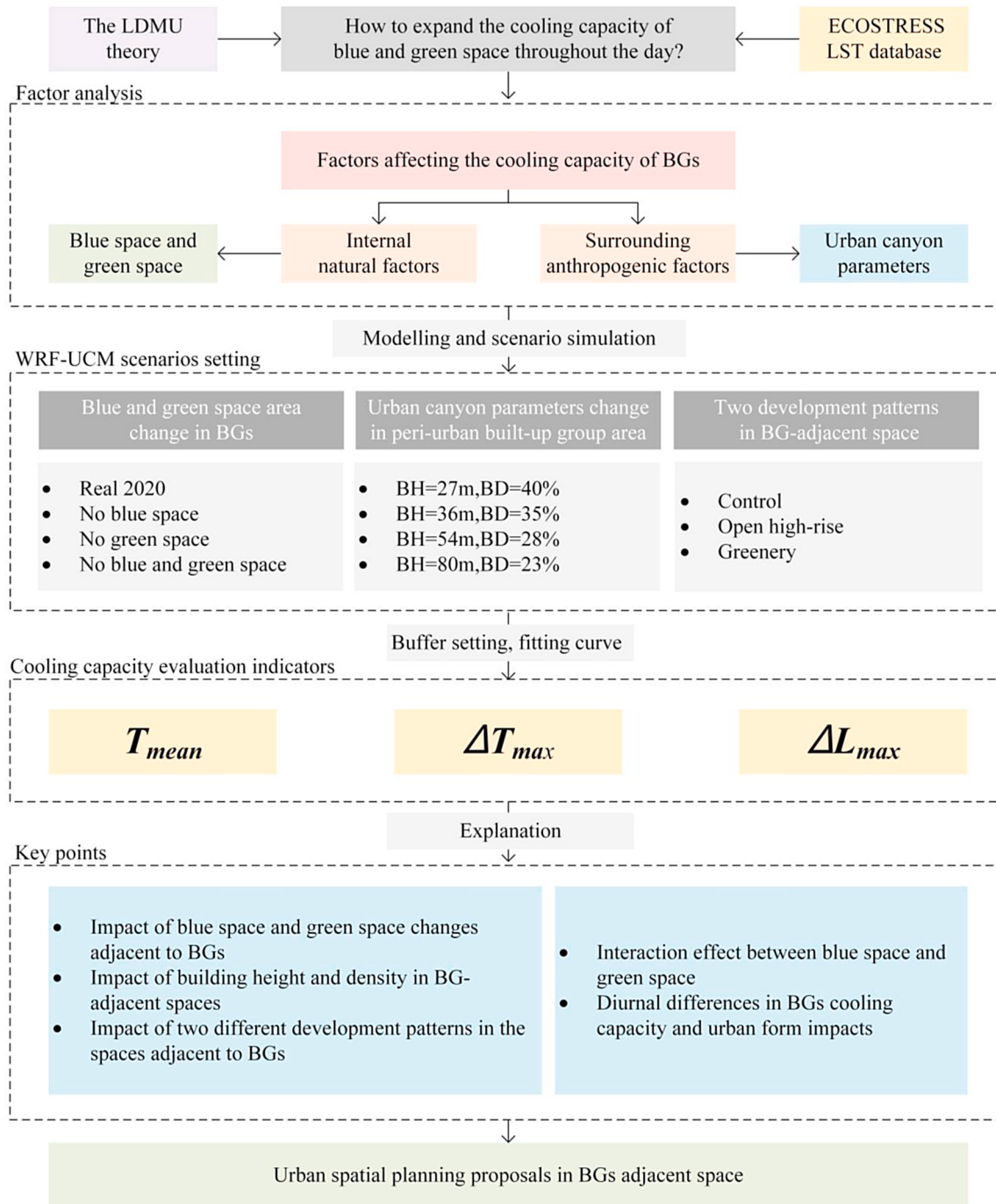


Fig. 1. Framework of this research.

area is after October 2022. Due to the influence of summer rainy weather on the quality of satellite images in the Wuhan area, we selected the LSTs obtained at 1:59 a.m. on April 9, 2023, for analysis, and the three LST images were combined to obtain a complete nightly LST image of the study area. The local weather conditions are cloudy and sunny, with a force 3 wind from the southeast and temperatures of 12–25 °C throughout the day.

2.3. Statistical analysis

To observe the nightly LDMU phenomenon in adjacent spaces at night, ECOSTRESS LST data were used as the measured data. Origin and Symbolab software packages were used to plot the fitted curves and

calculate the turning points. As shown in Fig. 3(a), there are higher LSTs in urban–rural fringe areas than in city centres, and high LSTs are concentrated in industrial areas at night. There is a weak fluctuating upwards trend further from the boundary of the BGs within a range of 5 km (Fig. 3(b)), and the two temperature inflection points appeared 1.62 km (23.77 °C) and 4.38 km (23.95 °C) from the boundary of the BGs. The temperature difference between the temperature at the first temperature inflection point and the BGs boundary (X = 0) is approximately 0.83 °C.

Referring to previous studies and observed nocturnal LSTs, BGs adjacent to the space cooling effect fitting curve were established (Yu et al., 2017; Zhu et al., 2021; Cai et al., 2022). Fig. 4(a) and (b) show three-dimensional hypothetical conceptual maps and fitted curves of temperature versus distance around BGs during the day and night,

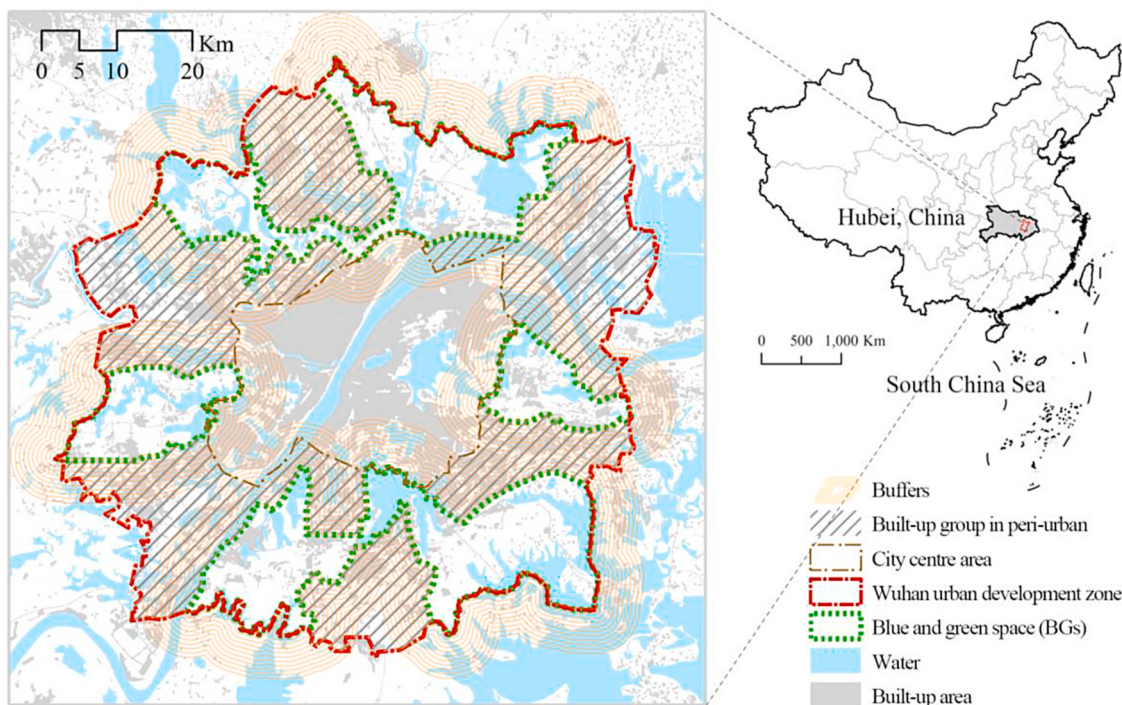


Fig. 2. Study area.

respectively. Ten buffers spaced 500 m apart around the BGs were created, where 5 buffers close to the BGs were defined as the spaces adjacent to the BGs (2.5 km). A curvilinear S-shaped curve (LDMU phenomenon) is shown in Fig. 4, with one inflection point during the day and two inflection points during the night at a range of 5 km; only the first turning point is discussed in this paper. To accurately quantify the mathematical relationship between the air temperature and distance in the adjacent space of the BGs, three and five mathematical fitting curves are created for daytime and night-time, respectively, where y is the air temperature at 2 m, x is the distance from the BGs, ΔL_{max} is the horizontal distance between the point of maxima P and point O, and ΔT_{max} is the difference in temperature between point P and the point of temperature difference at point O on the boundary of the BGs. In addition, we defined the average temperature across the 10 buffers as T_{mean} , and considering a lower T_{mean} for the buffer zones and larger ΔT_{max} and ΔL_{max} values is reasonable for assessing the cooling capacity of the BGs.

2.4. WRF-UCM model and case setting

This article utilizes the integrated WRF-UCM model with a local climate zone (LCZ) (Fig. 5). The urban canyon parameters for the different LCZ types are set as shown in Table 1 and are based on urban morphology data from Wuhan (Fig. S1) and the procedure in a previous work (Xu and Chen, 2021). The FRC_URB value is derived from the percentage of urban built-up land in the LUCC data, and other parameters, such as the aspect ratio and anthropogenic heat level, are set according to the descriptions of the different LCZ types (Stewart and Oke, 2012). The model adopts three-layer nesting ($4.5 \text{ km} \times 1.5 \text{ km} \times 0.5 \text{ km}$), simulating the period from July 6th to July 16th, 2022. The simulated data from the last three days are compared with the observed data from meteorological stations to evaluate the model performance. The ten established scenarios are shown in Table 2. Case 0 represents the current situation in 2020, focusing on the urban development zone. The blue and green areas on the map represent the planned boundaries of the six planned green wedges in Wuhan city, which are equivalent to the BGs concept in this article. The grey area in the middle represents the

city centre area, and the white area represents the non-built-up land. Within urban development zones, white areas outside the central city are built-up clusters to be developed. Rapid urbanization in Wuhan is typified by a reduction in the area of water bodies and degradation of croplands (Zhou et al., 2014; Ding and Chen, 2022a,b). Therefore, the green and blue spaces discussed in this paper refer to croplands and water within BGs, respectively. In Case 1, the water bodies within the BGs are transformed into soil (barren or sparsely vegetated, 16). In Case 2, the croplands within the BGs are converted into soil surfaces. In Case 3, the blue and green spaces within the BGs are converted into soil.

In May 2022, the Wuhan Natural Resources and Planning Bureau issued the *Opinions on Further Strengthening the Intensity Management of Residential Land Construction in Wuhan City*. According to this policy, the height of residential buildings within peri-urban built-up areas should not exceed 80 m, and the FAR should not exceed 2.5. Based on this regulation, the urban canyon parameters for Case 4 to Case 7 were set by maintaining the maximum plot ratio of 2.5 and altering the heights of the residential buildings. According to the *Standard for Urban Residential Area Planning and Design GB50180-2018*, the building heights were set at 27 m, 36 m, 54 m, and 80 m, following the specifications for multistory and high-rise buildings. To discuss the potential impact of spatial planning schemes on expansions in the cooling capacity of BGs, Case 8 and Case 9 were established. Based on the determined adjacent space of the BGs not exceeding 2.5 km in Case 0, while maintaining the same plot ratio, the strategies of increasing the greenery rate and changing the development mode from compact low-rise to open high-rise were implemented in these cases. Considering that certain urban spatial development needs are met, possible measures to enhance the permeability of BG benefits include increasing vegetation coverage and optimizing spatial forms. The various parameters can be modified in the URBPARM_LCZ. The TBL files were activated in the namelist.input program in WRF-UCM.

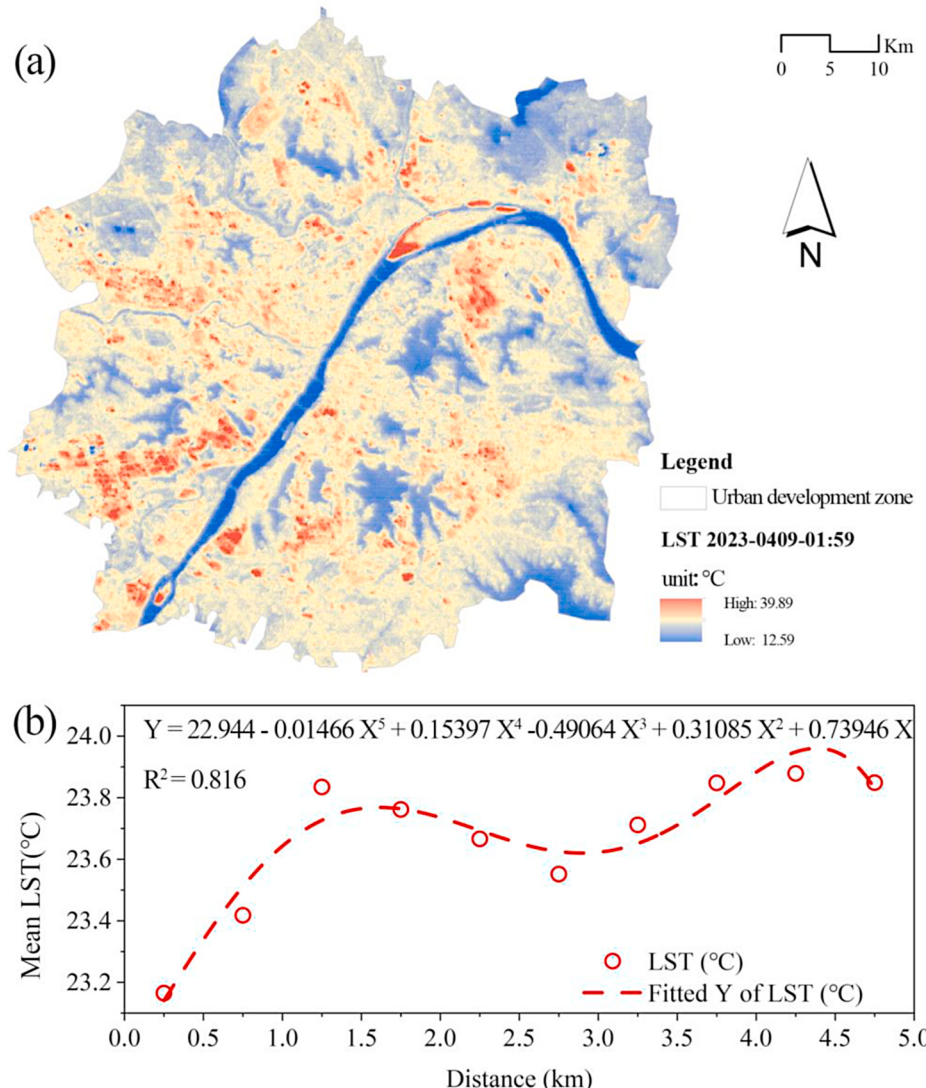


Fig. 3. Night-time LST in Wuhan. (a) Distribution of night-time LST; (b) night-time LST change based on distance from BG boundaries.

3. Results

3.1. Model evaluation

As shown in Fig. 6, the near-surface air temperature and wind speed simulated with the WRF-UCM model for 6 consecutive days for a total of 144 h (July 10 to July 15, 2022) are in good agreement with the measured values. The RMSE values of the measured and simulated air temperatures at the HD-Q1054 (114.33E, 30.58 N), CX-Q1015 (114.19E, 30.57 N), and HP-51491 (114.40E, 30.87 N) sites are 0.94 °C, 0.96 °C, and 0.78 °C, respectively. The RMSE values of the measured and simulated wind speeds are 1.29 m/s, 1.32 m/s, and 1.56 m/s, respectively. The measured and modelled values follow the same trend and exhibit diurnal differences. Based on the wind speed validation results of other scholars that applied WRF models, for which the RMSE was between 0.9 and 4.12 m/s (Arghavani et al., 2019; Chen et al., 2021; Li et al., 2022; Li et al., 2022; Vinayak et al., 2022), we consider the model performance to be acceptable.

3.2. Impact of blue space and green space changes adjacent to BGs

A comparison of the temperature profiles of the BG-adjacent spaces for the different scenario groups during the day (15:00) and night (3:00)

is shown in Fig. 7. Overall, there is a clear S-shaped profile for both BG-adjacent spaces during the day, and the difference between the scenarios becomes significant at night. In Case 0, the ΔL_{max} and ΔT_{max} of the peri-urban BGs in Wuhan are 2.15 km and 1.44 °C, respectively. Fig. 7(a) and (b) show the effect of the presence or absence of blue and green spaces inside the BGs on the cooling capacity of the BGs during the day (15:00) and night (3:00), respectively. Based on the obtained fitting equations (Table S1), the temperatures and distances of the inflection points were calculated. Table 3 shows that during the day, among the four scenarios, in the Case 0 (Real, 2020) scenario, ΔT_{max} (1.44 °C) and ΔL_{max} (2.15 km) are the largest, and T_{mean} (35.62 °C) is the lowest. At night, among the four scenarios, the Real 2020 ΔL_{max} (1.74 km) is the largest, T_{mean} (29.58 °C) is the lowest, and ΔT_{max} is 1.44 °C. The results of the numerical simulations corroborate the findings of the LST data. There are two temperature inflection points in adjacent spaces for both night-time BGs. The cooling distance ΔL_{max} of the BGs at night ranged from 1.4 to 1.7 km, and ΔT_{max} ranged from 0.21 to 0.7 °C. During day and night, the T_{mean} of the no blue and green space scenarios is maximized in all four scenarios, which shows that BGs are very effective in terms of their peripheral cooling ability throughout the day. During the daytime period, no green space can obtain larger ΔT_{max} and ΔL_{max} values.

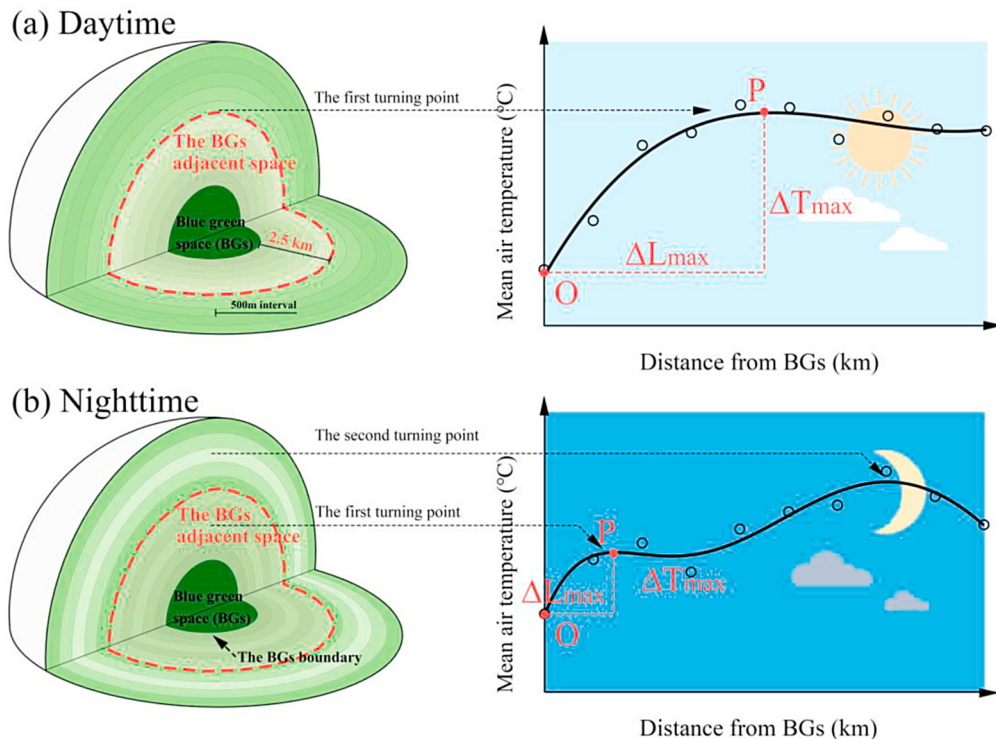


Fig. 4. Schematic of buffer setting and cooling effect fitting curves for BG-adjacent spaces.

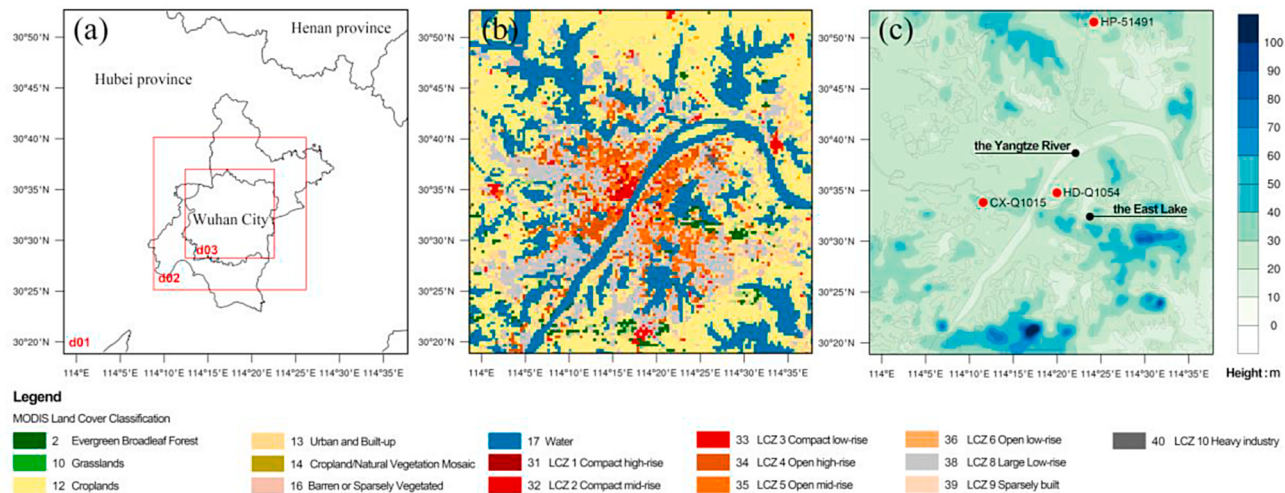


Fig. 5. Nested domain setting in the WRF-UCM model; (b) Land use map used for the d03 domain; (c) terrain height for the d03 domain and weather stations.

Table 1

Urban canyon parameter settings in the WRF-UCM model.

LCZ type	Urban fraction	Building density (%)	Building height (m)	Building width (m)	Road width (m)	Standard Deviation of roof height (m)
LCZ1	0.97	45	15.8	8.72	7.90	21
LCZ2	0.94	46	16.2	12.71	11.57	13.38
LCZ3	0.92	26	13.3	5.56	11.8	7.57
LCZ4	0.76	51	16.9	6.35	16.9	14.3
LCZ5	0.84	27	15.3	19.32	29.1	10.93
LCZ6	0.74	10	13.2	4.68	24.1	6.73
LCZ8	0.82	14	12.4	12.73	62.2	6.27
LCZ9	0.78	11	5.7	11.22	32.5	2.43
LCZ10	0.82	19	14	15.09	38.9	8.23

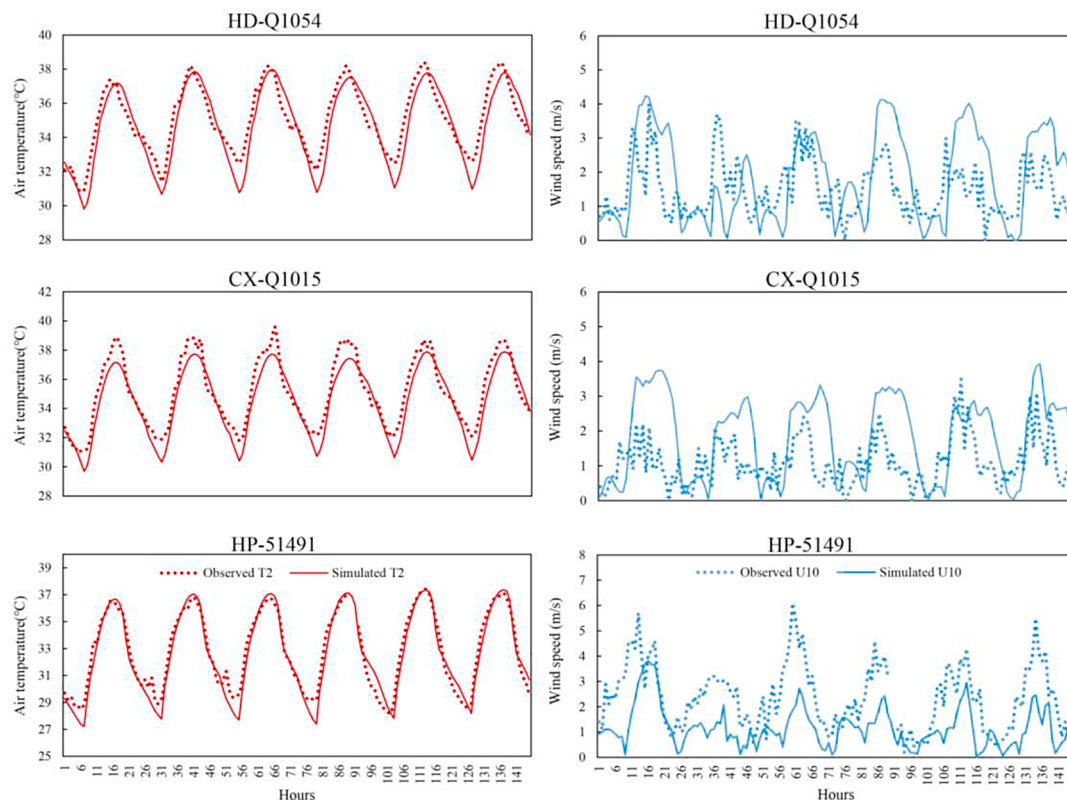
3.3. Impact of building height and density in BG-adjacent spaces

As shown in Fig. 7(c) and (d) and Table 4, open high-rises have a greater cooling advantage during the day, and compact low-rises perform better at night. During the day, Case 7 has a lower Tmean than Case 4 by 0.14 °C but larger ΔL_{max} and ΔT_{max} (0.07 km and 0.09 °C, respectively). At night, Case 4 has a lower Tmean of 0.24 °C, a lower ΔT_{max} of 0.09 °C and a larger ΔL_{max} of 0.315 km than does Case 7. The Tmean for Case 5 is between Case 4 and Case 7. Throughout the day, ΔT_{max} is consistently the largest for Case 7 (0.25°C–1.13 °C) and the smallest for Case 4 (0.16°C–1.04 °C). In addition, the difference in Tmean between compact low-rise buildings and open high-rise buildings was greater at night. Although the fitted curve does not capture the P point of Case 6 within 2.5 km, the four curves clearly have similar

Table 2

Schematic description of the case setting.

Case0 With blue & green space, the current situation in 2020	Case1 No blue space, the blue space changes to 16 (Barren)	Case2 No green space, the green space changes to 16	Case3 No blue & green space, the blue space and green space change to 16	Case4 Based on Case0, BH = 27 m, BD = 40 % (no anthropogenic heat) in built-up groups of peri-urban
Case5 Based on Case4, BH = 36 m, BD = 35 %	Case6 Based on Case4, BH = 54 m, BD = 28 %	Case7 Based on Case4, BH = 80 m, BD = 23 %	Case8 Open high-rise, based on Case4, BH changes from 27 m to 54 m, BD changes from 40 % to 28 % in BG-adjacent spaces	Case9 Greenery, based on Case4, green cover ratio changes from 24 % to 48 % in BG-adjacent spaces

**Fig. 6.** Comparison of observations and simulations at three weather stations.

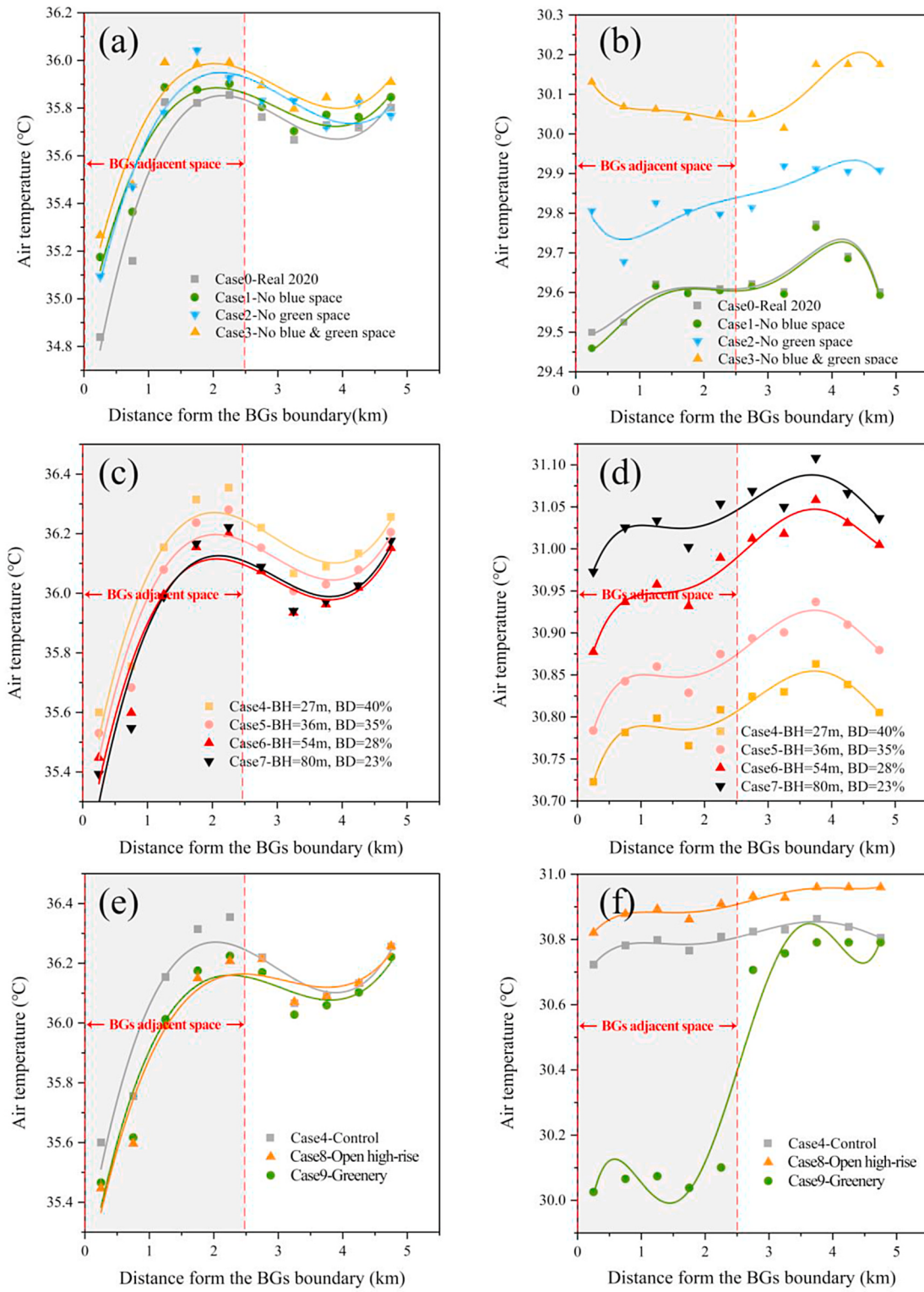


Fig. 7. Relationship between temperature and distance for different scenarios within 5 km of BGs at 15:00 during the day (a, c, and e) and 3:00 at night (b, d, and f).

characteristics.

3.4. Impact of two different development patterns in the spaces adjacent to BGs

As shown in Fig. 7(e) and (f) and Table 5, both the greenery and open high-rise strategies in the adjacent space of the BGs during the day are able to reduce Tmean. Compared to those in Case 4 (control scenario),

both Case 8 and Case 9 significantly reduce the temperature at point P by approximately 0.1 $^{\circ}\text{C}$, and ΔL_{\max} increases by 0.23 km and 0.42 km, respectively. At night, the effect of the greenery strategy is enhanced. Compared to that in the control scenario, Tmean within the adjacent space of the BGs in Case 8 is reduced by 0.52 $^{\circ}\text{C}$. Although the Case 8 scenario has a smaller ΔT_{\max} (0.14 $^{\circ}\text{C}$) than the Control scenario at night, the Tmean is relatively elevated by 0.1 $^{\circ}\text{C}$. The greenery strategy is more effective at cooling the spaces adjacent to the BGs throughout

Table 3Impact of BGs on indicators under different land use scenarios (units: ΔT , Tmean, °C; ΔL , km).

Case	Daytime (15:00)			Night-time (3:00)		
	ΔT_{max}	ΔL_{max}	T _{mean}	ΔT_{max}	ΔL_{max}	T _{mean}
Case0, Real 2020	1.44	2.15	35.62	0.21	1.74	29.57
Case1, No blue space	1.05	2.05	35.71	0.22	1.73	29.56
Case2, No green space	1.19	2.12	35.71	-	-	29.83
Case3, No blue & green space	1.06	2.02	35.80	-	-	30.07

* A deeper green colour indicates a lower T_{mean} and larger ΔT_{max} and ΔL_{max} .* A deeper green colour indicates a lower T_{mean} and larger ΔT_{max} and ΔL_{max} .**Table 4**Impact of different BD and BH parameters on various indicators in the built-up group throughout the diurnal cycle (units: ΔT , Tmean, °C; ΔL , km).

Case	Daytime (15:00)			Night-time (3:00)		
	ΔT_{max}	ΔL_{max}	T _{mean}	ΔT_{max}	ΔL_{max}	T _{mean}
Case4, BH=27 m, BD=40%	1.04	2.03	36.10	0.16	0.96	30.78
Case5, BH=36 m, BD=35%	1.03	2.05	36.03	0.17	0.95	30.84
Case6, BH=54 m, BD=28%	1.03	2.07	35.95	-	-	30.94
Case7, BH=80 m, BD=23%	1.13	2.10	35.95	0.25	0.64	31.02

* A deeper green colour indicates a lower T_{mean} and larger ΔT_{max} and ΔL_{max} .* A deeper green colour indicates a lower T_{mean} and larger ΔT_{max} and ΔL_{max} .**Table 5**Impact of different development patterns on indicators in BG-adjacent spaces throughout the diurnal cycle (units: ΔT , Tmean, °C; ΔL , km).

Case	Daytime (15:00)			Night-time (3:00)		
	ΔT_{max}	ΔL_{max}	T _{mean}	ΔT_{max}	ΔL_{max}	T _{mean}
Case 4, Control	1.04	2.03	36.10	0.16	0.96	30.78
Case 8, Open high-rise	1.05	2.45	36.02	0.14	0.93	30.87
Case 9, Greenery	1.04	2.26	36.01	-	-	30.06

* A deeper green colour indicates a lower T_{mean} and larger ΔT_{max} and ΔL_{max} values.* A deeper green colour indicates a lower T_{mean} and larger ΔT_{max} and ΔL_{max} values.

the day. While the open high-rise pattern is able to expand the cooling capacity of the BGs during the day, it substantially increases the T_{mean} within the adjacent space of the BGs at night. Additionally, Fig. 7(f) shows that the temperature is approximately 0.6 °C lower than that in the other two scenarios in the adjacent spaces of the BGs. Vegetation results in more latent heat dissipation, less heat is stored at the surface during the day, and night-time temperatures are much cooler than those in built-up areas.

4. Discussion

4.1. Interaction effect between blue space and green space

Different combinations of green space and blue space occurrences within the BGs have different cooling impacts on the peri-urban built-up group. As shown in Table 6, the cooling benefit of both blue spaces on the built-up group was significant during the day and at night, with a cooling capacity of approximately 0.17 °C during the day (with green space) and a maximum of 0.26 °C at night (without green space). The cooling benefit of green space for the build-up group occurred mainly at night. The maximum cooling capacity was 0.44 °C (without blue space), which was slightly lower during the day (when combined with blue space, the maximum cooling capacity was approximately 0.13 °C). There may be an interaction effect between green space and blue space within BGs. 2 (blue space: with, without) \times 2 (green space: with, without) repeated-measures ANOVA (Table 7) on temperature in the built-up groups showed a significant main effect of temperature in the built-up groups. During the daytime, the presence of blue space and green space in the BGs was more significant for cooling in the built-up groups, and there was a meaningful interaction ($\eta_p^2 > 0.01$, meaning that the independent variable had a significant effect on the dependent variable). Green space is most important for cooling the surroundings at

Table 6

Mean temperature within the build-up group for the different scenarios within the BGs (unit, °C).

	With blue space & with green space	With blue space & without green space	Without blue space & with green space	Without blue space & without green space
Daytime	35.70 ± 2.21	35.83 ± 2.17	35.87 ± 2.14	35.92 ± 2.30
Night-time	29.49 ± 1.67	29.64 ± 1.70	29.46 ± 1.67	29.90 ± 1.67

Table 7
Repeated measures ANOVA statistics.

Source	DF	Daytime (15:00)					Night-time (3:00)					
		AdjSS	AdjMS	F	P	η_p^2	AdjSS	AdjMS	F	P	η_p^2	
Main	Blue space	1	109.688	109.688	302.656	0.000	0.047	79.613	79.613	761.799	0.000	0.110
	Green space	1	50.212	50.212	381.790	0.000	0.058	527.337	527.337	2228.739	0.000	0.266
Interaction	Blue space & Green space	1	11.107	11.107	43.085	0.000	0.007	127.339	127.339	1170.953	0.007	0.160

Notes: SS, sum of squares; MS, mean squares.

night ($\eta_p^2 = 0.266$). There was a significant interaction effect between the presence of blue space and green space at night. The presence of blue space has a cooling effect of 0.26 °C on the surroundings during the night when green space disappears within the BGs. However, when green space is present in the BGs, the addition of blue space has a weak warming effect (0.03 °C) on the surrounding environment. In other words, the cooling effect of the water body is not obvious. The water body dissipates heat at night, the foliage of the vegetation may cause a blockage of heat emission from the surface, and there may be less heat accumulation at the surface than in the absence of forest. This further corroborates the findings of scholars (Yao et al., 2023) regarding the warming of water bodies at night.

4.2. Diurnal differences in BG cooling capacity and urban form impacts

At night, vegetation transpiration decreases, and the water body starts to release heat. The BG cooling capacity generally decreases, and ΔT_{max} and ΔL_{max} decrease. As Table 8 shows, for Case 0, ΔT_{max} is 1.44 °C during the day, 0.21 °C at night (85.8 % reduction), and ΔL_{max} is 2.15 km during the day, while it decreases to 1.74 km at night (19 % reduction). Compared to those in Case 0, in Case 1, the ratio of T_{max} decreased, and the decreases in ΔT_{max} and ΔL_{max} decreased. This suggests that the adverse effects of night-time heat release from water bodies cause a decrease in night-time air temperature in the surrounding area, as well as a decrease in the distance of penetration of the cooling air (Yao et al., 2023). In addition, there is a linear relationship between the changes in BD and BH within the peri-urban built-up group and the ΔT_{max} around the BGs, with the open high-rise mode having a smaller difference in ΔT_{max} between day and night than the compact low-rise mode; although shading of the open high-rise makes temperatures lower during the day, the difficulty of heat dissipation from the street

canyons during the night creates high temperatures (Ali-Toudert and Mayer, 2007; Hang and Chen, 2022). The built-up development construction in the built-up group contributed at least 33.8 % of the decline in the night-time ΔL_{max} , and the open high-rise pattern decreased the diurnal ΔT_{max} . However, changing from the compact low-rise pattern to open high-rise patterns only in the adjacent space of BGs can bring about a larger diurnal temperature difference (-16.5 %) in this space, and ΔT_{max} and ΔL_{max} at night will be smaller.

4.3. Implications for decision-making related to planning BG-adjacent spaces

According to the Wuhan Municipal Bureau of Statistics, the urban population of Wuhan in 2021 was more than 80 %, and most of these people lived within the city centre area. Therefore, peri-urban development must consider its impact on the microclimate of urban areas. Case 4 (Control) is used as the baseline scenario, and two thermal mitigation measures, Case 8 (open high-rise) and Case 9 (greenery), are implemented in the adjacent spaces of BGs. As shown in Fig. 8(d), the open high-rise measure significantly increased the night-time air temperature in the central city, with a localized warming of 0.3 °C (which exceeded 0.6 °C in the adjacent space of BGs). Although this process has a cooling effect on the adjacent spaces of BGs, it greatly increases the night-time temperature in the city centre area, making the process ill-advised. Zhang et al. observed the LST in Wuhan in different seasons and reported that the summer LST in LCZ 4 was lower than that in LCZ 3 during the daytime but became hotter at night (Zhang et al., 2022). Wang et al. also reported that taller buildings have hotter LSTs at night (Wang et al., 2023). Moreover, this research further showed that the high-rise and low-density forms still cannot prevent this warming phenomenon. In the evening, the greenery measure had a good cooling effect on the temperatures in the upwind BG adjacent space and in the city centre area. In addition, downwind greenery has a significant cooling effect (above 1 °C) for neighbourhoods with enhanced greenery. The local cooling benefits of downwind upgrading greenery measures are significant, while the warming effects of high-rise and low-density patterns are no longer significant.

An interesting phenomenon can be seen in Fig. 8(d). First, at night in the downwind (southerly) area, the greenery strategy results in more than 0.6 °C of cooling in the interior of the implementation area, while the cooling effect is smaller in the interiors of the upwind and downwind BG-adjacent spaces. Second, the diffusion effect of the cooling air in the upwind area is obvious and creates a cooling effect in a certain peripheral area, but the cooling of the surrounding area is limited in the downwind area. This is because urban heat waves are transported by the wind to downwind regions, suburban winds are similar in temperature to upwind BG-adjacent spaces, and hot winds from urban areas have higher temperatures than downwind BG adjacent spaces.

Unlike the relatively sparse urban sprawl in Austin, USA (Zhao et al., 2020), and the low-rise and dense sprawl in four cities in Spain (Domingo et al., 2023), Chinese megacities such as Wuhan (Ding and Chen, 2022a,b) and Shanghai (Cai et al., 2022) have experienced the emergence of an open high-rise process in peri-urban areas. Notably, open high-rise urbanization in peri-urban areas exacerbates night-time heat-waves in central urban areas. To mitigate the impact of the deterioration of the thermal environment in the city centre during the peri-urban

Table 8
Diurnal differences in the BG cooling capacity index.

Case name	Night-time ΔT_{max} change rate compared to daytime	Night-time ΔL_{max} change rate compared to daytime	Night-time T_{max} change rate compared to daytime
Case0, Real 2020	-85.8 %	-19.0 %	-17.0 %
Case1, No blue space	-78.8 %	-15.9 %	-17.2 %
Case4, BH = 27 m, BD = 40 %	-84.5 %	-52.8 %	-14.7 %
Case5, BH = 36 m, BD = 35 %	-83.9 %	-53.5 %	-14.4 %
Case7, BH = 80 m, BD = 23 %	-78.1 %	-69.4 %	-13.7 %
Case8, Open high-rise	-86.4 %	-62.3 %	-16.5 %

*Cases 2, 3, 6, and 9 were not counted due to inconsistent trends in the fitted curves.

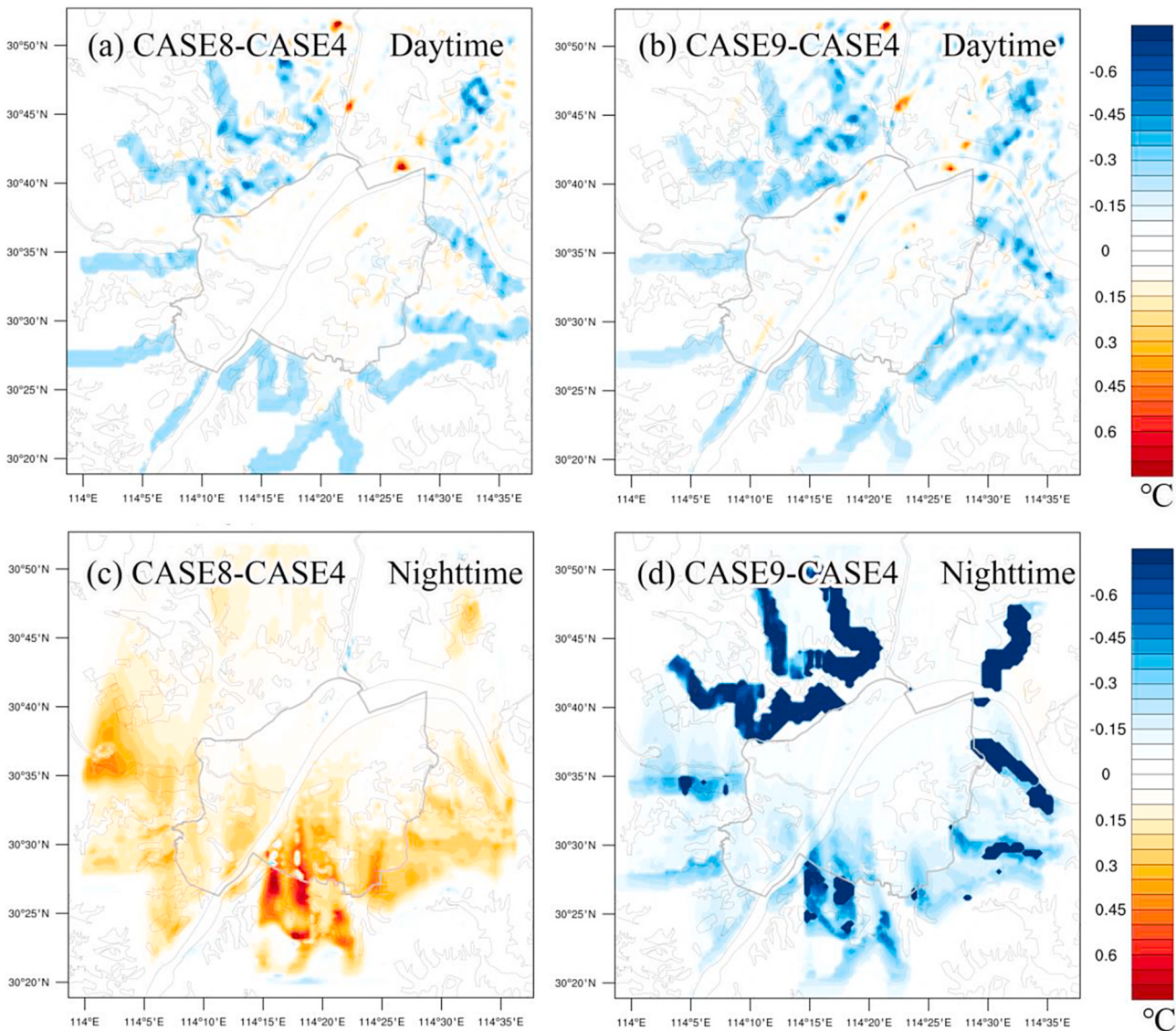


Fig. 8. Diurnal effects of different development patterns on air temperature in the city centre area in BGs adjacent space.

development process, natural-based solutions such as enhancing the street greening rate and adding rooftop greening in peri-urban residential communities may be feasible for coping with heatwaves in the city centre (Khan et al., 2023).

4.4. Limitations and future work

Additional work needs to be carried out in the future. First, the controlled experiment in this paper focused on the impact of spatial morphological changes and did not consider AH emissions or pollutant emissions. In the spatial structure of many cities, industrial zones are usually close to city centres, and some scholars suggest that industrial zones be located in suburbs far from cities (Wu et al., 2021). However, the spatial layout of peri-urban land, which is a typical land use type, and its spatial planning of adjacent spatial measures have not been fully discussed. In the future, the spatial planning of adjacent spaces will be explored as a climate regulation strategy for high anthropogenic heat and pollutant emission industrial land use in peri-urban areas. Second, because this study concluded that a single wind direction is the main contributing factor, future scenarios with multiple wind directions should be established. In fact, the wind direction dominates the area affected by heatwaves. Han et al. expressed the same concern when

discussing the dispersion of pollutants: when the concentration of pollutants in suburban areas is greater than that in city centre areas, urban ventilation corridors will exacerbate air pollution in central urban areas (Han et al., 2022). During the construction of ventilation corridors, in addition to improvements in the ventilation performance of the site, attention should be given to whether possible heat or pollution sources may adversely affect the city centre via suburban winds. Finally, “the second turning point” and “the distance between the first and second turning points” are very interesting topics, but due to the limited distance between the BGs in this paper, it was not possible to further explore these topics; however, they will be explored in the future.

Compared to the simulated air temperature at 2 m above the surface, this paper finds that the inverted LST obtained with the aid of satellites underestimates the ΔL_{max} and overestimates the ΔT_{max} of the BGs. The cooling distance of the BGs at night in the real case, ΔL_{max} , ranges between 1.4 (LST) and 1.7 (simulated air temperature) km, and ΔT_{max} ranges between 0.21 (simulated air temperature) and 0.7 (LST) °C. Despite the outstanding advantages of satellite remote sensing inversion of night-time LSTs in terms of high data resolution, large period coverage, and rapid analysis, this method is strongly dependent on local weather conditions. For this reason, we were not able to obtain daytime LSTs comparable to night-time LSTs in this study. We will continue to

pay attention to the relevant diurnal and all-day LST inversion products in the future and carry out an in-depth comparative study.

5. Conclusion

In this study, we used the ECOSTRESS LST and the validated WRF-UCM model to determine the diurnal and nocturnal cooling distances and cooling intensity of peri-urban BGs. The effects of internal blue-green space, BD and BH, different development patterns and greening rates in the spaces adjacent to the BGs on their cooling capacity were also discussed. The following conclusions were obtained.

The ΔL_{max} and ΔT_{max} of the peri-urban BGs in Wuhan were 2.15 km and 1.44 °C, respectively; the cooling capacity of the BGs generally weakened in the evening, and ΔT_{max} and ΔL_{max} decreased. The LDMU phenomenon was not observed when there was no green space in the BGs. The implementation of the open high-rise development pattern while maintaining a certain FAR was able to expand the ΔL_{max} during the daytime, but a large amount of heat was released during the night-time, resulting in an increase in the adjacent space of the BGs and the temperature of the city centre. The night-time compact low-rise model had a larger ΔL_{max} and lower T_{mean} and performed better at expanding the cooling capacity of the BGs and lowering the temperature in the city centre. In addition, the greenery strategy had a significant effect on lowering the temperature in the adjacent space of the BGs and in the city centre at night and could increase ΔL_{max} during the daytime and reduce ΔT_{max} and T_{mean} . Both greenery and open high-rise systems reduced the temperature at the first turning by approximately 0.2 °C. Built-up development construction in all peri-urban built-up group regions contributed at least 33.8 % of the decline in night-time ΔL_{max} .

The urban morphology parameters of BGs adjacent to built-up spaces can modulate the BG cooling capacity, but the diurnal variability in climate impacts needs to be assessed. Open high-rise areas aid in expanding BG cooling during the day, and compact low-rise areas display better cooling at night, with lower average temperatures than other areas. Enhancements in greenness are generally effective. This study showed that a city can utilize this natural advantage to alleviate environmental problems such as heat islands. Whether it is a water body or a green space, other cities, such as Nanjing and Nanchang, can exploit the ideas in this paper to propose nature-based solutions. The research results in this paper can guide the development and construction of peri-urban ventilation corridors around planning areas during the rapid expansion process and can provide urban heat wave mitigation ideas for governments and urban planners in different climate zones.

CRediT authorship contribution statement

Wei Ding: Writing – original draft, Visualization, Validation, Software, Methodology, Investigation, Funding acquisition, Conceptualization. **Mengyang Liu:** Writing – review & editing, Methodology. **Yunni Wu:** Writing – review & editing, Conceptualization. **Hong Chen:** Writing – review & editing, Supervision, Project administration, Funding acquisition.

Declaration of competing interest

The authors declare that they have no known competing financial interests or personal relationships that could have appeared to influence the work reported in this paper.

Data availability

Data will be made available on request.

Acknowledgements

This study is supported by the National Natural Science Foundation of China (No. 51778251 & 51538004) and the Fundamental Research Funds for the Central Universities, HUST (No. 2022JYCXJJ065). Numerical computations were performed at the Hefei Advanced Computing Center.

Appendix A. Supplementary data

Supplementary data to this article can be found online at <https://doi.org/10.1016/j.jclepro.2024.141165>.

References

- Ali-Toudert, F., Mayer, H., 2007. Effects of asymmetry, galleries, overhanging façades and vegetation on thermal comfort in urban street canyons. *Sol. Energy* 81 (6), 742–754.
- Arghavani, S., Malakooti, H., Bidokhti, A.A., 2019. Numerical evaluation of urban green space scenarios effects on gaseous air pollutants in Tehran Metropolis based on WRF-Chem model. *Atmos. Environ.* 214, 116832.
- Bernard, J., Rodler, A., Morille, B., Zhang, X., 2018. How to design a park and its surrounding urban morphology to optimize the spreading of cool air? *Climate* 6 (1), 10.
- Cai, Z., Demuzere, M., Tang, Y., Wan, Y., 2022a. The characteristic and transformation of 3D urban morphology in three Chinese mega-cities. *Cities* 131, 103988.
- Cai, Z., Guldmann, J.-M., Tang, Y., Han, G., 2022b. Does city-water layout matter? Comparing the cooling effects of water bodies across 34 Chinese megacities. *J. Environ. Manag.* 324, 116263.
- Cao, J., Zhou, W., Yu, W., Hu, X., Yu, M., Wang, J., Wang, J., 2022. Urban expansion weakens the contribution of local land cover to urban warming. *Urban Clim.* 45, 101285.
- Chen, B., Wang, W., Dai, W., Chang, M., Wang, X., You, Y., Zhu, W., Liao, C., 2021. Refined urban canopy parameters and their impacts on simulation of urbanization-induced climate change. *Urban Clim.* 37, 100847.
- Cheung, P.K., Livesley, S.J., Nice, K.A., 2021. Estimating the cooling potential of irrigating green spaces in 100 global cities with arid, temperate or continental climates. *Sustain. Cities Soc.* 71, 102974.
- Ding, W., Chen, H., 2022a. Urban-rural fringe identification and spatial form transformation during rapid urbanization: a case study in Wuhan, China. *Build. Environ.*, 109697.
- Ding, W., Chen, H., 2022b. Urban-rural fringe identification and spatial form transformation during rapid urbanization: a case study in Wuhan, China. *Build. Environ.* 226, 109697.
- Domingo, D., Van Vliet, J., Hersperger, A.M., 2023. Long-term changes in 3D urban form in four Spanish cities. *Landsc. Urban Plann.* 230, 104624.
- Fang, Y., Zhao, L., 2022. Assessing the environmental benefits of urban ventilation corridors: a case study in Hefei, China. *Build. Environ.* 212, 108810.
- Feng, W., Ding, W., Zhen, M., Zou, W., Wang, H., 2022. Cooling effect of urban small green spaces in Qujiang Campus, Xi'an Jiaotong University, China. *Environ. Dev. Sustain.* 24 (3), 4278–4298.
- Fisher, J.B., Lee, B., Purdy, A.J., Halverson, G.H., Dohlen, M.B., Cawse-Nicholson, K., Wang, A., Anderson, R.G., Aragon, B., Arain, M.A., 2020. ECOSTRESS: NASA's next generation mission to measure evapotranspiration from the international space station. *Water Resour. Res.* 56 (4), e2019WR026058.
- Ghosh, S., Das, A., 2018. Modelling urban cooling island impact of green space and water bodies on surface urban heat island in a continuously developing urban area. *Model. Earth Syst. Environ.* 4 (2), 501–515.
- Guo, F., Zhao, J., Zhang, H., Dong, J., Zhu, P., Lau, S.S.Y., 2023. Effects of urban form on sea cooling capacity under the heatwave. *Sustain. Cities Soc.* 88, 104271.
- Han, D., An, H., Cai, H., Wang, F., Xu, X., Qiao, Z., Jia, K., Sun, Z., An, Y., 2023. How do 2D/3D urban landscapes impact diurnal land surface temperature: insights from block scale and machine learning algorithms. *Sustain. Cities Soc.* 99, 104933.
- Han, L., Zhao, J., Zhang, T., Zhang, J., 2022. Urban ventilation corridors exacerbate air pollution in central urban areas: evidence from a Chinese city. *Sustain. Cities Soc.* 87, 104129.
- Hang, J., Chen, G., 2022. Experimental study of urban microclimate on scaled street canyons with various aspect ratios. *Urban Clim.* 46, 101299.
- Hong, C., Wang, Y., Gu, Z., 2023. How to understand the heat island effects in high-rise compact urban canopy? *City Built Environ.* 1 (1), 2.
- Khan, A., Carlesena, L., Khorat, S., Khatun, R., Das, D., Doan, Q.-V., Hamdi, R., Aziz, S. M., Akbari, H., Santamouris, M., 2023. Urban cooling potential and cost comparison of heat mitigation techniques for their impact on the lower atmosphere. *Comput. Urban Sci.* 3 (1), 26.
- Li, H., Yuan, F., Shen, L., Liu, Y., Zheng, Z., Zhou, X., 2022. Improving the WRF/urban modeling system in China by developing a national urban dataset. *Geosci. Front.* 13 (4), 101385.
- Li, L., Zhu, A., Huang, L., Wang, Q., Chen, Y., Ooi, M.C.G., Wang, M., Wang, Y., Chan, A., 2022. Modeling the impacts of land use/land cover change on meteorology and air quality during 2000–2018 in the Yangtze River Delta region, China. *Sci. Total Environ.* 829, 154669.

- Liu, R., Han, Z., Li, J., Li, J., Liang, L., Wu, Y., 2023. The impacts of urban anthropogenic heat and surface albedo change on boundary layer meteorology and air pollutants in the Beijing-Tianjin-Hebei region. *Urban Clim.* 47, 101358.
- Mohan, M., Kikegawa, Y., Gurjar, B.R., Bhati, S., Kolli, N.R., 2013. Assessment of urban heat island effect for different land use–land cover from micrometeorological measurements and remote sensing data for megacity Delhi. *Theor. Appl. Climatol.* 112, 647–658.
- Ouyang, W., Morakinyo, T.E., Ren, C., Ng, E., 2020. The cooling efficiency of variable greenery coverage ratios in different urban densities: a study in a subtropical climate. *Build. Environ.* 174, 106772.
- Peng, J., Dan, Y., Qiao, R., Liu, Y., Dong, J., Wu, J., 2021. How to quantify the cooling effect of urban parks? Linking maximum and accumulation perspectives. *Remote Sens. Environ.* 252, 112135.
- Ren, C., Yang, R., Cheng, C., Xing, P., Fang, X., Zhang, S., Wang, H., Shi, Y., Zhang, X., Kwok, Y.T., 2018. Creating breathing cities by adopting urban ventilation assessment and wind corridor plan—The implementation in Chinese cities. *J. Wind Eng. Ind. Aerod.* 182, 170–188.
- Ren, J., Shi, K., Kong, X., Zhou, H., 2023. On-site measurement and numerical simulation study on characteristic of urban heat island in a multi-block region in Beijing, China. *Sustain. Cities Soc.* 95, 104615.
- Shi, M., Chen, M., Jia, W., Du, C., Wang, Y., 2023. Cooling effect and cooling accessibility of urban parks during hot summers in China's largest sustainability experiment. *Sustain. Cities Soc.* 93, 104519.
- Stewart, I.D., Oke, T.R., 2012. Local climate zones for urban temperature studies. *Bull. Am. Meteorol. Soc.* 93 (12), 1879–1900.
- Sun, R., Chen, A., Chen, L., Liu, Y., 2012. Cooling effects of wetlands in an urban region: the case of Beijing. *Ecol. Indicat.* 20, 57–64.
- Vinayak, B., Lee, H.S., Gedam, S., Latha, R., 2022. Impacts of future urbanization on urban microclimate and thermal comfort over the Mumbai metropolitan region, India. *Sustain. Cities Soc.* 79, 103703.
- Wang, Q., Wang, X., Meng, Y., Zhou, Y., Wang, H., 2023. Exploring the impact of urban features on the spatial variation of land surface temperature within the diurnal cycle. *Sustain. Cities Soc.* 91, 104432.
- Wang, Y., Berardi, U., Akbari, H., 2016. Comparing the effects of urban heat island mitigation strategies for Toronto, Canada. *Energy Build.* 114, 2–19.
- Wong, N.H., Yu, C., 2005. Study of green areas and urban heat island in a tropical city. *Habitat Int.* 29 (3), 547–558.
- Wu, S., Chen, C., Wang, Y., Yu, Z., Cao, J., Zhang, R., Song, H., 2021. Differential effects of valley city morphology on mesoscale flow field characteristics. *Build. Environ.* 205, 108283.
- Wu, Y., Chen, H., 2023. Optimizing block morphology for reducing traffic pollutant concentration in adjacent external spaces of street canyons: a machine learning approach. *Build. Environ.* 242, 110587.
- Xu, H., Chen, H., 2021. Impact of urban morphology on the spatial and temporal distribution of PM_{2.5} concentration: a numerical simulation with WRF/CMAQ model in Wuhan, China. *J. Environ. Manag.* 290, 112427.
- Yao, L., Sailor, D.J., Zhang, X., Wang, J., Zhao, L., Yang, X., 2023. Diurnal pattern and driving mechanisms of the thermal effects of an urban pond. *Sustain. Cit. Soc.*, 104407.
- Yao, X., Yu, K., Zeng, X., Lin, Y., Ye, B., Shen, X., Liu, J., 2022. How can urban parks be planned to mitigate urban heat island effect in “Furnace cities”? An accumulation perspective. *J. Clean. Prod.* 330, 129852.
- Yu, C., Hien, W.N., 2006. Thermal benefits of city parks. *Energy Build.* 38 (2), 105–120.
- Yu, K., Chen, Y., Liang, L., Gong, A., Li, J., 2020. Quantitative analysis of the interannual variation in the seasonal water cooling island (WCI) effect for urban areas. *Sci. Total Environ.* 727, 138750.
- Yu, Z., Guo, X., Jørgensen, G., Vejre, H., 2017. How can urban green spaces be planned for climate adaptation in subtropical cities? *Ecol. Indicat.* 82, 152–162.
- Zhang, L., Nikolopoulou, M., Guo, S., Song, D., 2022. Impact of LCZs spatial pattern on urban heat island: a case study in Wuhan, China. *Build. Environ.* 226, 109785.
- Zhang, Q., Zhou, D., Xu, D., Rogora, A., 2022. Correlation between cooling effect of green space and surrounding urban spatial form: evidence from 36 urban green spaces. *Build. Environ.* 222, 109375.
- Zhang, X., Feng, T., Zhao, S., Yang, G., Zhang, Q., Qin, G., Liu, L., Long, X., Sun, W., Gao, C., 2021. Elucidating the impacts of rapid urban expansion on air quality in the Yangtze River Delta, China. *Sci. Total Environ.* 799, 149426.
- Zhang, Y., Gu, Z., 2013. Air quality by urban design. *Nat. Geosci.* 6 (7), 506–506.
- Zhao, C., Weng, Q., Hersperger, A.M., 2020. Characterizing the 3-D urban morphology transformation to understand urban-form dynamics: a case study of Austin, Texas, USA. *Landsc. Urban Plann.* 203, 103881.
- Zhou, X., Ooka, R., Chen, H., Kawamoto, Y., Kikumoto, H., 2014. Impacts of inland water area changes on the local climate of Wuhan, China. *Indoor Built Environ.* 25 (2), 296–313.
- Zhou, X., Zhang, S., Liu, Y., Zhou, Q., Wu, B., Gao, Y., Zhang, T., 2022. Impact of urban morphology on the microclimatic regulation of water bodies on waterfront in summer: a case study of Wuhan. *Build. Environ.* 226, 109720.
- Zhu, W., Sun, J., Yang, C., Liu, M., Xu, X., Ji, C., 2021. How to measure the urban park cooling island? A perspective of absolute and relative indicators using remote sensing and buffer analysis. *Rem. Sens.* 13 (16), 3154.